

1 Electrical properties of Si/diamond heterojunction diodes fabricated by using surface activated bonding

2 Yota Uehigashi<sup>1</sup>, Shinya Ohmagari<sup>2,3</sup>, Hitoshi Umezawa<sup>3</sup>, Hideaki Yamada<sup>3</sup>, Jianbo Liang<sup>1,4</sup>, and Naoteru

3 Shigekawa<sup>1,4\*</sup>

4 <sup>1</sup>*Graduate School of Engineering, Osaka City University, 3-3-138 Sugimoto, Sumiyoshi, Osaka 558-8585,*

5 *Japan*

6 <sup>2</sup>*Sensing Material Research Team, Sensing System Research Center, National Institute of Advanced*

7 *Industrial Science and Technology, 807-1 Shukumachi, Tosu, Saga 841-0052, Japan.*

8 <sup>3</sup>*Diamond Wafer Team, Advanced Power Electronics Research Center, National Institute of Advanced*

9 *Industrial Science and Technology, 1-8-31 Midorigaoka, Ikeda, Osaka 563-8577, Japan*

10 <sup>4</sup>*Graduate School of Engineering, Osaka Metropolitan University, 3-3-138 Sugimoto, Sumiyoshi, Osaka 558-*

11 *8585, Japan*

12 \*E-mail: shigekawa@omu.ac.jp

13  
14 We evaluated the current–voltage ( $I$ – $V$ ) and temperature-dependent  $I$ – $V$  characteristics of n<sup>+</sup>-Si/p-diamond  
15 heterojunction diodes (HDs) fabricated by using surface activated bonding and Ru/p-diamond Schottky barrier  
16 diodes (SBDs). Both types of diodes were fabricated on diamond surface that was activated using a fast atom  
17 beam of Ar. Their room-temperature reverse-bias characteristics were explained using the trap-assisted  
18 tunneling model, wherein the surface activation process affects the carrier transport across the Si/diamond and

1 Ru/diamond interfaces. In addition, we compared the electrical properties of n<sup>+</sup>-Si/p-diamond HDs and Ru/p-  
2 diamond SBDs with those of previously fabricated p<sup>+</sup>-Si/p-diamond HDs and Al/p-diamond SBDs. A  
3 correlation between the barrier heights and the work function of the contact materials (n<sup>+</sup>-Si, p<sup>+</sup>-Si, and Ru)  
4 was observed.  
5

## 1 **1. Introduction**

2 Diamond is the most promising material for fabricating high-power, high-temperature, and radiation-  
3 resistant semiconductor devices because of its outstanding electronic properties: a breakdown field of  $>10$   
4  $\text{MV cm}^{-1}$ , high electron and hole mobilities  $>2000 \text{ cm}^2 \text{ V}^{-1}\text{s}^{-1}$ , saturated drift velocities as high as  $2.5 \times 10^7$   
5  $\text{cm s}^{-1}$  for electrons and  $1.4 \times 10^7 \text{ cm s}^{-1}$  for holes and high displacement energy (43 eV/atom) [1–5].  
6 However, the energy levels of phosphorus (P) and nitrogen (N), typical n-type dopants for diamond, are too  
7 deep ( $\sim 0.57$  and  $1.7$  eV below the conduction band edge, respectively) for them to be efficiently activated at  
8 room temperature; this limits the applications of diamond to electronic devices [6,7]. Establishment of pn  
9 junctions is the key for producing diamond-based devices such as bipolar transistors and junction field effect  
10 transistors. A possible method of solving this problem is to use direct bonding technologies, such as surface  
11 activated bonding (SAB), in which samples are bonded to each other without heating after their bonding  
12 surfaces are activated by using a fast atom beam (FAB) [8–11]. Si/diamond [12,13], GaAs/diamond [14], and  
13  $\beta\text{-Ga}_2\text{O}_3$ /diamond [15] heterojunction diodes (HDs) were previously fabricated by direct bonding. In  
14 particular, we previously fabricated  $\text{p}^+\text{-Si/p-diamond}$  HDs using SAB and investigated the band structure of  
15 Si/diamond bonding interfaces [12]. In addition, we demonstrated that  $\text{p}^+\text{-Si/p-diamond}$  HDs were more  
16 stable against thermal processing than Al/p-diamond and Cu/p-diamond Schottky barrier diodes (SBDs)  
17 [16,17]. However, there is not enough research on carrier transport at Si/diamond interfaces.

1 In this study, we evaluated the characteristics of n<sup>+</sup>-Si/p-diamond HDs and Ru/p-diamond SBDs and  
2 compared their properties with those of previously fabricated p<sup>+</sup>-Si/p-diamond HDs [12] and Al/p-diamond  
3 SBDs [16] to investigate the electrical properties of Si/diamond interfaces.

4

## 5 **2. Experimental methods**

6 A B-doped drift layer and 7- $\mu\text{m}$ -thick metal-assisted termination (MAT) buffer layer [18,19] ( $[\text{B}] \sim 5 \times 10^{20}$   
7  $\text{cm}^{-3}$ ,  $[\text{W}] \sim 1 \times 10^{19} \text{ cm}^{-3}$ ) were epitaxially grown on a B-doped HPHT diamond (100) substrate ( $[\text{B}] \sim 1 \times 10^{18}$   
8  $\text{cm}^{-3}$ ). The B concentration in the drift layer was estimated to be  $1 \times 10^{16} \text{ cm}^{-3}$  from cathodoluminescence spectra  
9 [20,21]. The net concentration of ionized acceptors in the drift layer ( $N_a^- - N_d^+$ , where  $N_a^-$  and  $N_d^+$  are the  
10 concentrations of ionized acceptors and donors, respectively) was estimated to be  $6.5 \times 10^{13} \text{ cm}^{-3}$  from  
11 capacitance-voltage characteristics. We also prepared a silicon-on-insulator (SOI) substrate that was composed  
12 of a 6.5- $\mu\text{m}$ -thick heavily ( $\sim 10^{19} \text{ cm}^{-3}$ ) Sb-doped device layer, a 1- $\mu\text{m}$ -thick SiO<sub>2</sub> layer, and a Si (100) substrate.  
13 The surface of the diamond drift layer was mechanically polished. The thickness of the drift layer ( $W_{\text{drift}}$ ) was  
14 estimated to be 20  $\mu\text{m}$  after polishing. The average roughness (Ra) measured using an atomic force microscope  
15 was 0.3 and 0.1 nm for the diamond and Si surfaces, respectively. The device layer of the SOI substrate was  
16 bonded to the diamond drift layer by using SAB. Next, the Si substrate and SiO<sub>2</sub> layer were removed by  
17 grinding and wet etching to fabricate an n<sup>+</sup>-Si/p-diamond heterojunction. We made n<sup>+</sup>-Si mesas by wet etching  
18 and formed contacts on the back of the diamond substrate and the surface of the Si mesas by evaporating Ti/Au

1 multi layers. After forming the Si/diamond junctions, the uncovered diamond surface was terminated by  
2 oxygen by irradiating it with ultraviolet light in an oxygen atmosphere [22,23]. The SBDs were fabricated by  
3 evaporating Ru/Au multilayers as Schottky contacts on the diamond drift layer. A schematic cross section of  
4 the fabricated diodes is shown in Fig. 1. Note that the HDs and SBDs were fabricated on the same diamond  
5 substrate. We performed sequential post-process annealing on the fabricated diodes (703 K for 30 min and 873  
6 K for 30 min). The current-voltage ( $I$ - $V$ ) characteristics at room temperature and  $I$ - $V$  characteristics at ambient  
7 temperatures between 293 K and 473 K (the temperature-dependent  $I$ - $V$  characteristics) were measured for  
8 respective diodes in a vacuum after each annealing step. A source measure unit (Agilent B2902A, B1505A)  
9 was used for measurements of  $I$ - $V$  characteristics.

10

### 11 **3. Results**

12 The  $I$ - $V$  characteristics at room temperature for the  $n^+$ -Si/p-diamond HDs and Ru/p-diamond SBDs before  
13 and after annealing at 703 K and 873 K are shown in Figs. 2(a)-2(c). The  $I$ - $V$  characteristics of  $p^+$ -Si/p-diamond  
14 HDs [12] are also shown for comparison. We computed the ideality factor from the steepest part of each  $I$ - $V$   
15 curve between -1.7 and -0.7 V. We defined the reverse-bias current, turn-on voltage, and on/off ratio as the  
16 magnitude of the current at 3 V, the forward-bias voltage for a current of 1 mA/cm<sup>2</sup>, and the ratio of current at  
17 -3 V to that at +3 V, respectively. The  $I$ - $V$  characteristics of the  $n^+$ -Si/p-diamond HDs before annealing did not  
18 show diode characteristics, which is assumed to be attributable to (I) that the properties of ohmic contacts

1 formed on back of the p<sup>+</sup>-diamond substrate were poor and/or (II) that interface states were formed during the  
2 surface activation process [24,25]. The turn-on voltage of the n<sup>+</sup>-Si/p-diamond HDs was higher than that of  
3 the p<sup>+</sup>-Si/p-diamond HDs, which is due to the difference in band structure between these HDs. The parameter  
4 values for the respective annealing conditions are summarized in Table 1. The parameters of the Al/p-diamond  
5 SBDs [16] are also listed. The ideality factors of annealed HDs are close to that of annealed Ru/p-diamond  
6 HDs. The ideality factor of Ru/p-diamond SBDs decreased by annealing, which was in good contrast to the  
7 behavior of the ideality factor of Al/p-diamond SBD. The difference in the ideality factors between the two  
8 SBDs might be attributed to the thermal stability of Ru/diamond interfaces superior to that of Al/diamond  
9 interfaces [26,27]. In contrast to the Ru/p-diamond SBDs, the *I-V* characteristics of HDs annealed at 873 K  
10 show a hump around -1.4 V, which might be attributable to defects formed at annealed interfaces. A possible  
11 origin of such defects is (1) local strain and resultant deterioration in crystal quality at Si/diamond interfaces  
12 because of large difference in the coefficients of thermal expansion between Si and diamond ( $1.8 \times 10^{-6} \text{ }^\circ\text{C}^{-1}$ )  
13 [28] and (2) intermediate layers formed at Si/diamond interfaces during the annealing [29].

14 Figures 3(a) and 3(b) show the temperature-dependent *I-V* characteristics of the n<sup>+</sup>-Si/p-diamond HDs after  
15 annealing at 703 and 873 K while Figs. 3(c) and 3(d) show those of the Ru/p-diamond SBDs. The turn-on  
16 voltage decreased as the ambient temperature was increased. In contrast, no marked increase was observed in  
17 the reverse-bias current when the ambient temperature was changed.

18 The saturation current density  $J_s$  was obtained by extrapolating the forward-bias current density of each

1 curve to 0 V. Figure 4(a) shows the relationship between  $\ln(J_s/T^2)$  and  $1/k_B T$  (the Richardson plot) of the  $n^+$ -  
 2 Si/p-diamond HDs, Ru/p-diamond SBDs,  $p^+$ -Si/p-diamond HDs, [12] and Al/p-diamond SBDs [16] after  
 3 annealing at 703 K. The Richardson plots of these four diodes after annealing at 873 K are shown in Fig. 4 (b).  
 4 Here,  $k_B$  and  $T$  are the Boltzmann constant and ambient temperature, respectively. Using thermionic emission  
 5 (TE) model,  $J_s$  is expressed as

$$6 \quad J_s = A^* T^2 \exp\left(-\frac{qV_b}{k_B T}\right), \quad (1)$$

7 where  $A^*$ ,  $q$ , and  $qV_b$  are the Richardson constant, elementary charge, and barrier height, respectively. On the  
 8 basis of the TE model, we fitted the relationship between  $\ln(J_s/T^2)$  and  $1/kT$  to a straight line and estimated the  
 9 barrier height. The barrier heights were found to be 1.65, 1.28, 0.85, and 0.78 eV for the  $n^+$ -Si/p-diamond HDs,  
 10 Ru/p-diamond SBDs,  $p^+$ -Si/p-diamond HDs, and Al/p-diamond SBDs after annealing at 703 K, respectively.  
 11 Moreover, the barrier heights for the diodes after annealing at 873 K were found to be 1.2, 1.0, 0.55, and 0.55  
 12 eV, for the  $n^+$ -Si/p-diamond HDs, Ru/p-diamond SBDs,  $p^+$ -Si/p-diamond HDs, and Al/p-diamond SBDs,  
 13 respectively.

14 Figures 5(a) and 5(b) show the reverse-bias characteristics of the  $n^+$ -Si/p-diamond HDs and Ru/p-diamond  
 15 SBDs after annealing at 703 K and 873 K. Breakdown occurred at 1080 V in the  $n^+$ -Si/p-diamond HDs and at  
 16 420 V in the Ru/p-diamond SBDs after annealing at 703 K. The breakdown voltages after annealing at 873 K  
 17 were 420 and 110 V for the  $n^+$ -Si/p-diamond HDs and Ru/p-diamond SBDs, respectively. The deterioration of  
 18 reverse-bias characteristics for  $n^+$ -Si/p-diamond HDs after annealing at 873 K may be due to the formation of

1 defects at annealed Si/diamond interfaces, as was suggested for the origin of the hump formed around -1.4 V.  
 2 A deeper understanding of the origin of the degradation in characteristics of annealed HDs might be obtained  
 3 by systematically investigating nanostructural properties of annealed Si/diamond interfaces using methods  
 4 such as transmission electron microscopy.

5 Using the trap-assisted tunneling (TAT) model [30–32], the reverse-bias current density is expressed as

$$6 \quad J_{\text{TAT}} \propto \exp\left(-\frac{8\pi\sqrt{2qm^*}V_t^{3/2}}{3hE}\right) \quad (2).$$

7 Here,  $h$ ,  $E$ ,  $m^*$ , and  $qV_t$  are the Planck constant, electric field at the interface, effective mass of the carrier, and  
 8 trap energy level. We assumed that  $m^*$  was  $0.908 m_0$  [33], where  $m_0$  is the electron rest mass. The depletion  
 9 region thickness ( $W_{\text{depletion}}$ ) is given by

$$10 \quad W_{\text{depletion}} = \sqrt{\frac{2\varepsilon_{\text{dia}}\varepsilon_0}{qN_A}\left(V_{\text{bi}} + V - \frac{k_{\text{B}}T}{q}\right)} \quad (3)$$

11 where  $\varepsilon_0$ ,  $\varepsilon_{\text{dia}}$ ,  $V_{\text{bi}}$ , and  $V$  are the permittivity of the vacuum, dielectric constant of diamond, built-in potential,  
 12 and applied reverse-bias voltage, respectively. We set  $\varepsilon_{\text{dia}}$  at 5.7 [33].  $V_{\text{bi}}$  of the n<sup>+</sup>-Si/p-diamond HDs and  
 13 Ru/p-diamond SBDs after annealing at 703 K was estimated to be 1.27 and 0.87 V, respectively, from the  
 14 Richardson plots. Using Eq. (3), thickness of the depletion region was found to be larger than that of the drift  
 15 layer at a reverse-bias voltage of 1080 V, which implied that the drift layer was completely depleted. Thus,  $E$   
 16 was given by

$$17 \quad E = \frac{V+V_{\text{bi}}}{W_{\text{drift}}}. \quad (4)$$

18 Figures 5(c) and 5(d) shows the relationship between  $\ln(J)$  and  $1/E$  (TAT plot) [31,32], where  $J$  is the current

1 density, of the n<sup>+</sup>-Si/p-diamond HDs and Ru/p-diamond SBDs after annealing at 703 K and 873 K.  $qV_i$  was  
2 estimated to be 0.13, 0.08, and 0.03 eV for n<sup>+</sup>-Si/p-diamond HDs and Ru/p-diamond SBDs after annealing at  
3 703 K, and n<sup>+</sup>-Si/p-diamond HDs after annealing at 873 K, respectively, by fitting the measured reverse-bias  
4 characteristics using eq. (2). These  $qV_i$  values are slightly smaller than the reported depths of defects in CVD-  
5 grown diamond (0.2-1.7 eV) [34–39]. The reverse-bias characteristics of the Ru/p-diamond SBDs after  
6 annealing at 873 K were not explained using TAT model. The breakdown field for HDs and SBDs, which was  
7 estimated to be 0.5 and 0.2 MV/cm, respectively, was lower than the ideal breakdown field of diamond(7.7-20  
8 MV/cm) [40]. Noting that the breakdown field of SBDs with field plate (1.8 MV/cm) was reportedly higher  
9 than that of SBDs without field plate (0.8 MV/cm) [41], the breakdown field of HDs and SBDs may be  
10 increased by incorporating edge-termination techniques.

11 We also examined possibility of other models such as the thermionic emission (TE) model [42], TE model  
12 with barrier lowering effects considered (TE + BL model) [43], thermionic field emission (TFE) model [25],  
13 TFE model with barrier lowering effects considered (TFE + BL model) [44–47], and Poole-Frenkel emission  
14 (PFE) model [48,49] for explaining the reverse-bias characteristics of HDs and SBDs. No good fits were  
15 obtained using models other than TAT model.

16

#### 17 **4. Discussion**

18 Figure 6 shows the energy-band diagram of n<sup>+</sup>-Si/p-diamond HDs at reverse-bias voltage estimated by

1 assuming that no offset is formed in the vacuum level across n<sup>+</sup>-Si/p-diamond bonding interface. On this  
 2 assumption, the band offset for n<sup>+</sup>-Si/p-diamond HDs  $\Delta E_c$  and  $\Delta E_v$  is expressed as

$$3 \quad \Delta E_c = E_{g, \text{dia}} - qV_b - \delta_{n, \text{Si}}, \quad (5)$$

$$4 \quad \Delta E_v = E_{g, \text{dia}} - \Delta E_c - E_{g, \text{Si}}. \quad (6)$$

5 where  $E_{g, \text{dia}}$  ( $E_{g, \text{Si}}$ ) and  $\delta_{n, \text{Si}}$  are the bandgap energy of diamond (Si) and the difference between the Fermi level  
 6 and the conduction band minimum in n<sup>+</sup>-Si, respectively. We use  $E_{g, \text{Si}} = 1.12$  eV and  $E_{g, \text{dia}} = 5.47$  eV in the  
 7 literature [42]. We estimate  $\delta_{n, \text{Si}} = 0.03$  eV from the ionized acceptor concentration in the drift layer and effective  
 8 density of states in conduction band of Si. We assume that  $qV_b$  is 1.60 eV based on the analysis of the  
 9 Richardson plot. We find that  $\Delta E_c = 3.84$  eV and  $\Delta E_v = 0.51$  eV.

10 We previously reported that Ar FAB irradiation of surfaces led to the formation of amorphous-like layers at  
 11 the bonding interfaces of diamond/Si heterojunctions [50,51]. Given that the reverse-bias characteristics of the  
 12 n<sup>+</sup>-Si/p-diamond HDs and Ru/p-diamond SBDs were explained by TAT model, the current is assumed to be  
 13 due to the following two-step process (Fig. 6). First, holes are thermally excited to the trap states. Second, the  
 14 holes tunnel to the valence band of the p-diamond. Noting that a larger breakdown voltage was observed for  
 15 SBDs with higher Schottky barriers [52], the larger breakdown voltage of the n<sup>+</sup>-Si/p-diamond HDs than that  
 16 of the Ru/p-diamond SBDs is likely to be due to the higher barrier of the n<sup>+</sup>-Si/p-diamond interfaces. The  
 17 reverse-bias characteristics of typical SBDs fabricated using the conventional process were explained by the  
 18 TE and TFE+BL models [43–47], which is in good contrast to the present work. The difference in the features

1 of the reverse-bias characteristics suggests that the traps were also formed during the surface activation process  
2 of diamond and/or the Si surface, as was reported for p-Si/n-Si bonding interfaces [30]. Advanced  
3 characterization of bonding interfaces such as transient photo-response spectroscopy is expected to play an  
4 important role for clarifying their electrical properties [53–55].

5 Figure 7 shows the correlation between the barrier height estimated by the Richardson plot and the work  
6 functions of the contact materials (n<sup>+</sup>-Si, p<sup>+</sup>-Si, Ru, and Al). The S factors ( $S = \partial qV_b / \partial \chi_m$ , where  $\chi_m$  is the  
7 work function) of the Si/p-diamond HDs and Ru/p-diamond SBDs after annealing at 703 K and 873 K are  
8 close to 0.7 and 0.6, respectively. The measured barrier heights of the Al/p-diamond SBDs after annealing at  
9 703 K and 873 K are placed below lines for  $S=0.7$  and  $0.6$ , which is due to the thermal stability of Al/diamond  
10 interfaces inferior to those of Si/diamond and Ru/diamond interfaces [16,17,26,27]. The observed S factor  
11 close to 1, which is significantly larger than that reported for p-diamond SBDs fabricated on oxygen-terminated  
12 surfaces (0.47) [56], suggests formation of partially “pinning-free” interfaces in the present work. A possible  
13 explanation is that the Ar FAB irradiation partially removed the high-density oxygen-related surface states [57],  
14 which were assumed to pin the Fermi level at the diamond surface. The surface activation process of diamond  
15 by Ar FAB irradiation is assumed to play an important role of realizing its pinning-free surface. The  
16 controllability of performances of diamond-based devices such as turn-on voltage and breakdown  
17 characteristics might be enhanced by bonding diamond to materials with different work functions (such as  
18 semiconductors with different polarities) and fabricating pinning-free interfaces.

1

2

### 3 **5. Conclusion**

4 We fabricated n<sup>+</sup>-Si/p-diamond HDs and Ru/p-diamond SBDs on diamond surfaces activated using Ar FAB.

5 Their reverse-bias characteristics were explained by the TAT model, which suggested that traps were formed

6 during the surface activation process. The S factors of Si/diamond HDs and Ru/p-diamond SBDs after

7 annealing at 703 K and 873 K were close to 0.7 and 0.6, respectively. The correlation between the barrier

8 height and the work function of the contact materials (n<sup>+</sup>-Si, p<sup>+</sup>-Si, and Ru) suggested formation of partially

9 “pinning-free” interfaces in HDs and SBDs wherein the Ar FAB irradiation partially removed the high-density

10 oxygen-related surface states. These results imply that fabrication of diamond/semiconductor HDs by using

11 surface activated bonding is assumed to play an important role in promoting the development of diamond

12 devices.

13

### 14 **Acknowledgements**

15 This work was supported in part by a JSPS KAKENHI Grant No. 20K04581.

16

1 **Table I.** Ideality factor, reverse-bias current, turn-on voltage, rectification  
2 factor of n<sup>+</sup>-Si/p-diamond HDs, Ru/p-diamond SBDs, previously fabricated p<sup>+</sup>-Si/p-diamond HDs  
3 [12], and Al/p-diamond SBDs [16].

	Annealing temperature	Ideality factor	Reverse-bias Current (mA/cm <sup>2</sup> )	Turn-on voltage (V)	Rectification factor
n <sup>+</sup> -Si/p-diamond HDs	Before annealing	-	2.74	1.00	10 <sup>0</sup>
	703 K	1.20	1×10 <sup>-3</sup> -1×10 <sup>-2</sup>	1.56	10 <sup>4</sup>
	873 K	1.30	1×10 <sup>-3</sup> -1×10 <sup>-2</sup>	1.15	10 <sup>5</sup>
Ru/p-diamond SBDs	Before annealing	2.76	1×10 <sup>-3</sup> -1×10 <sup>-2</sup>	1.77	10 <sup>4</sup>
	703 K	1.38	1×10 <sup>-3</sup> -1×10 <sup>-2</sup>	1.56	10 <sup>4</sup>
	873 K	1.22	1×10 <sup>-3</sup> -1×10 <sup>-2</sup>	1.32	10 <sup>5</sup>
p <sup>+</sup> -Si/p-diamond HDs [12]	Before annealing	2.62	1.12	1.27	10 <sup>7</sup>
	703 K	1.85	1×10 <sup>-3</sup> -1×10 <sup>-2</sup>	1.38	10 <sup>7</sup>
	873 K	1.25	1×10 <sup>-3</sup> -1×10 <sup>-2</sup>	0.83	10 <sup>7</sup>
Al/p-diamond SBDs [16]	Before annealing	1.38	1×10 <sup>-3</sup> -1×10 <sup>-2</sup>	0.97	10 <sup>7</sup>
	703 K	1.37	1×10 <sup>-3</sup> -1×10 <sup>-2</sup>	0.96	10 <sup>7</sup>
	873 K	1.57	1×10 <sup>-3</sup> -1×10 <sup>-2</sup>	0.90	10 <sup>7</sup>

4

1 **Figure Captions**

2 **Fig. 1.** Schematic cross section of fabricated  $n^+$ -Si/p-diamond HDs and Ru/p-diamond SBDs.

3

4 **Fig. 2.**  $I$ - $V$  characteristics at room temperature for  $n^+$ -Si/p-diamond HDs, Ru/p-diamond SBDs, and  
5  $p^+$ -Si/p-diamond HDs [12] before annealing (a) and after annealing at 703 K (b) and 873 K (c).

6

7 **Fig. 3.** Temperature-dependent  $I$ - $V$  characteristics of  $n^+$ -Si/p-diamond HDs after annealing at 703 K  
8 (a) and 873 K (b). Temperature-dependent  $I$ - $V$  characteristics of Ru/p-diamond SBDs after  
9 annealing at 703 K (c) and 873 K (d).

10

11 **Fig. 4.** Relationship between  $J_s$  and  $1/k_B T$  (Richardson plot) of  $n^+$ -Si/p-diamond HDs, Ru/p-diamond  
12 SBDs,  $p^+$ -Si/p-diamond HDs [12], and Al/p-diamond SBDs [16] after annealing at 703 K (a) and 873  
13 K (b).

14

15 **Fig. 5.** Reverse-bias characteristics of  $n^+$ -Si/p-diamond HDs and Ru/p-diamond SBDs after annealing  
16 at 703 K (a) and 873 K (b). TAT plots of  $n^+$ -Si/p-diamond HDs and Ru/p-diamond SBDs after  
17 annealing at 703 K (c) and 873 K (d).

18

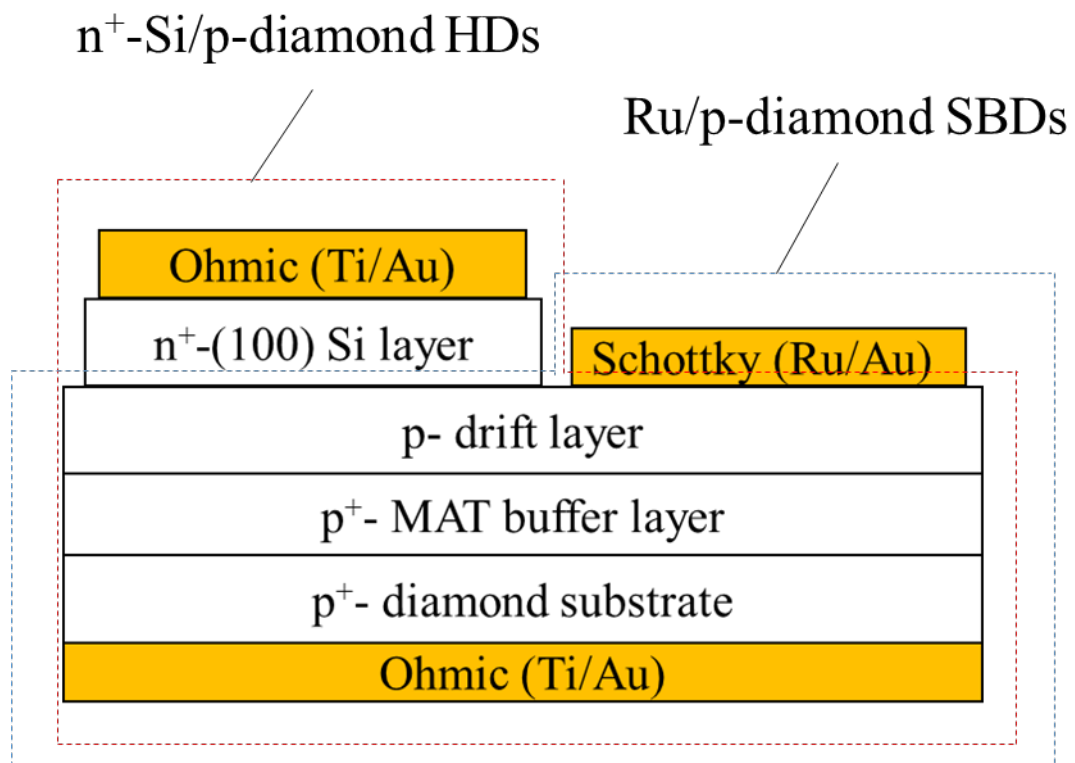
1 **Fig. 6.** Carrier transport of n<sup>+</sup>-Si/p-diamond interfaces under reverse bias.

2

3 **Fig. 7.** Correlation between barrier height estimated by Richardson plot and work function of contact

4 materials (n<sup>+</sup>-Si, p<sup>+</sup>-Si, Ru, and Al).

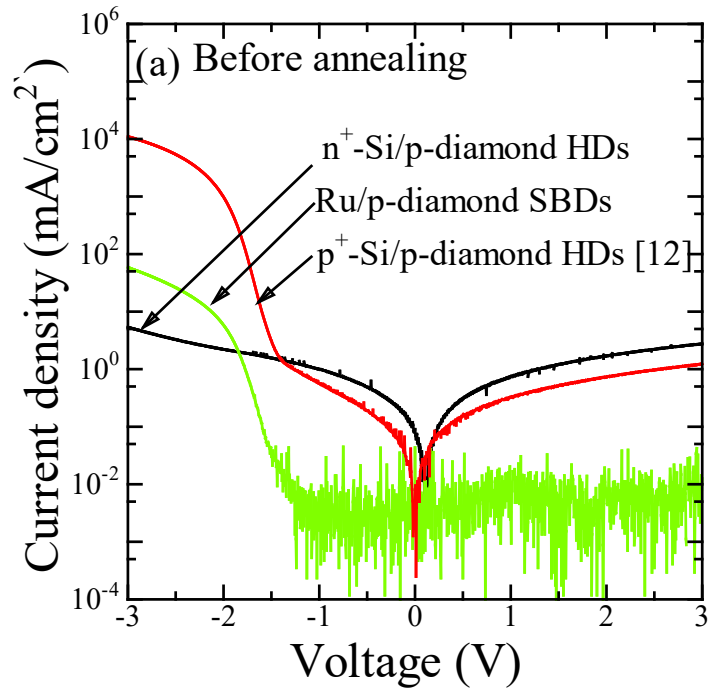
1 Fig. 1.



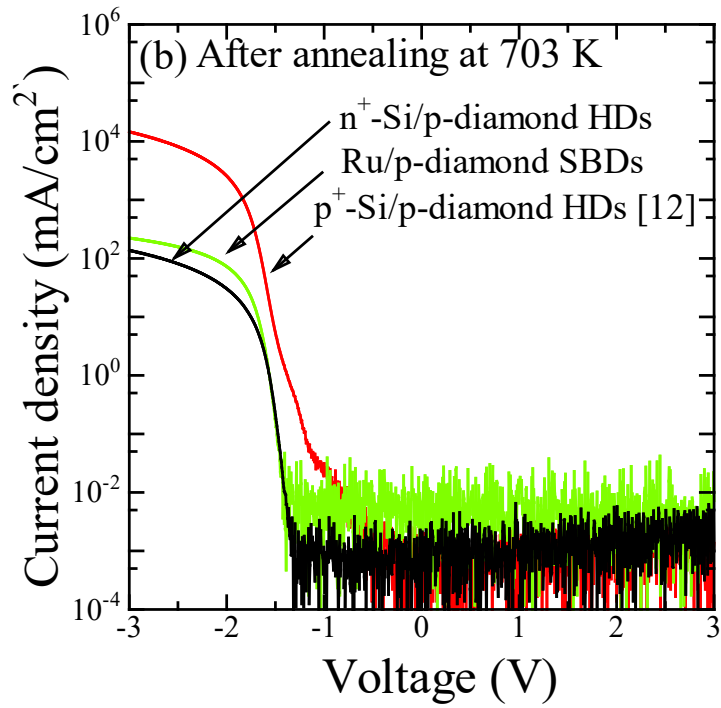
2

3

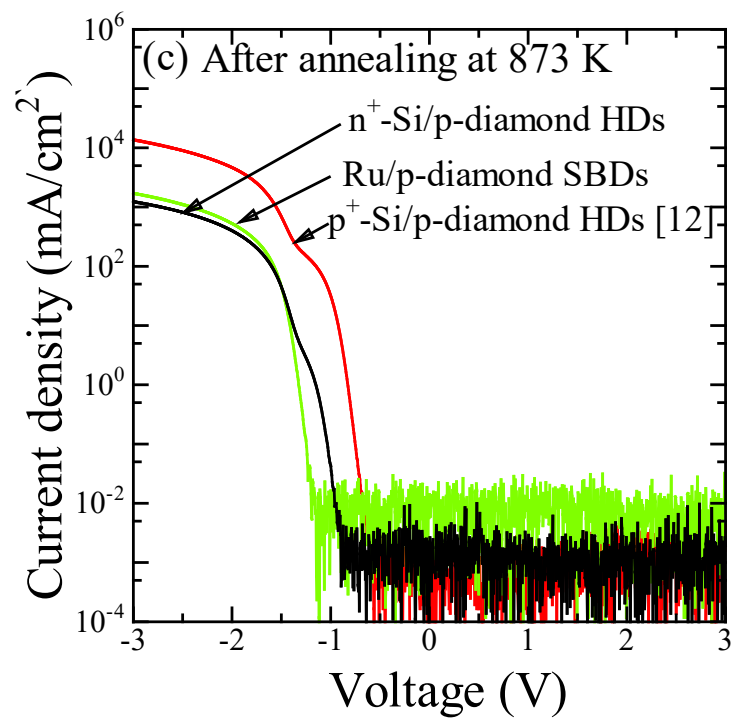
1 Fig. 2.



2



3

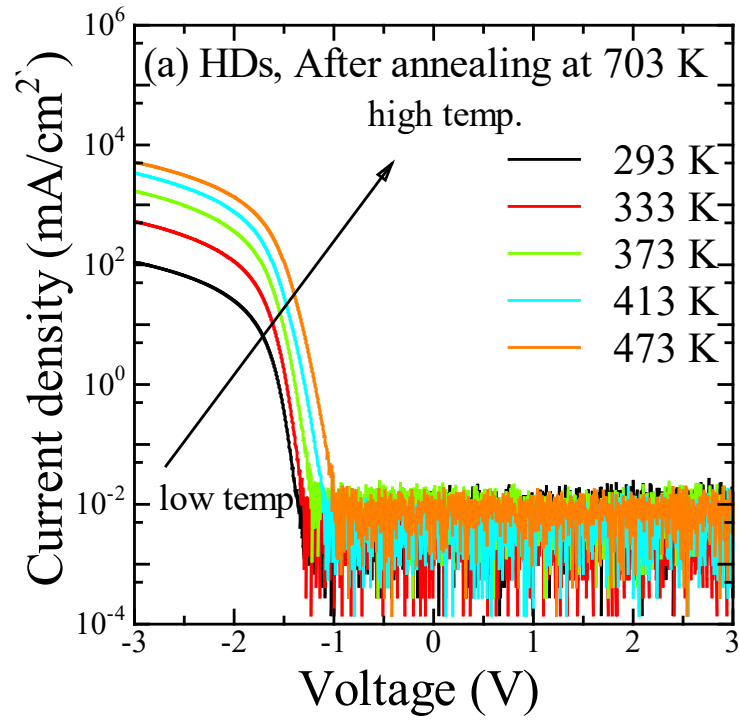


1

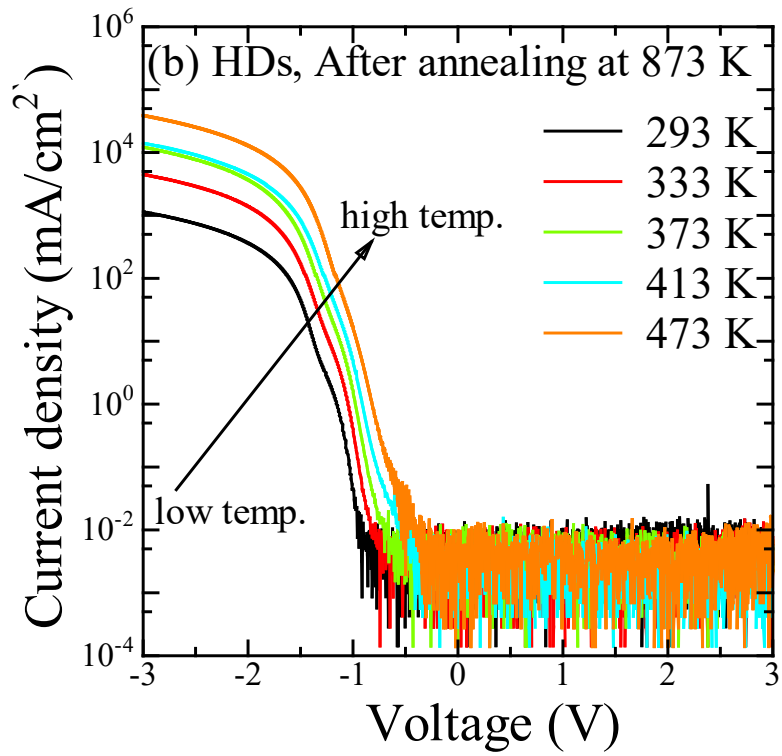
2

3

1 **Fig. 3.**

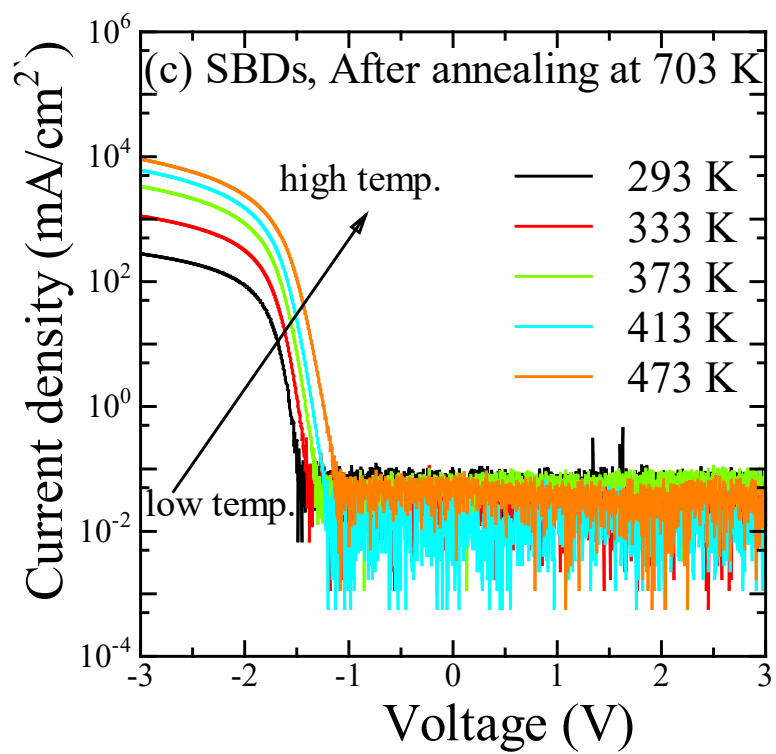


2

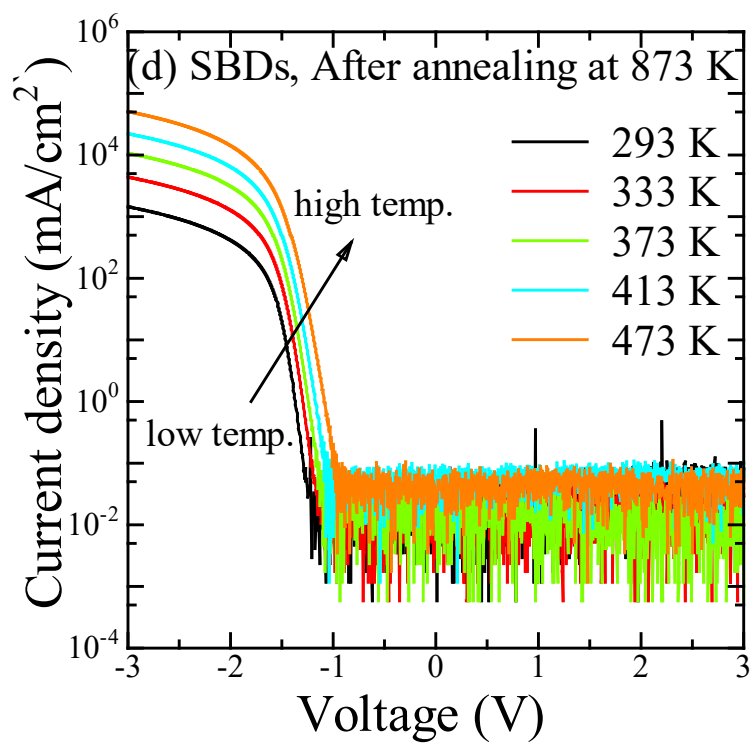


3

4



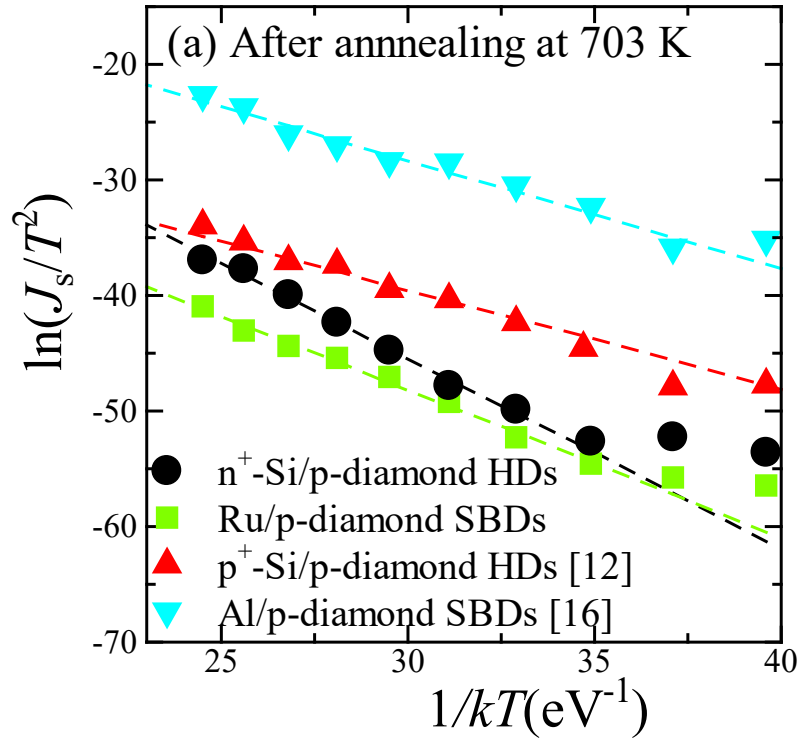
1



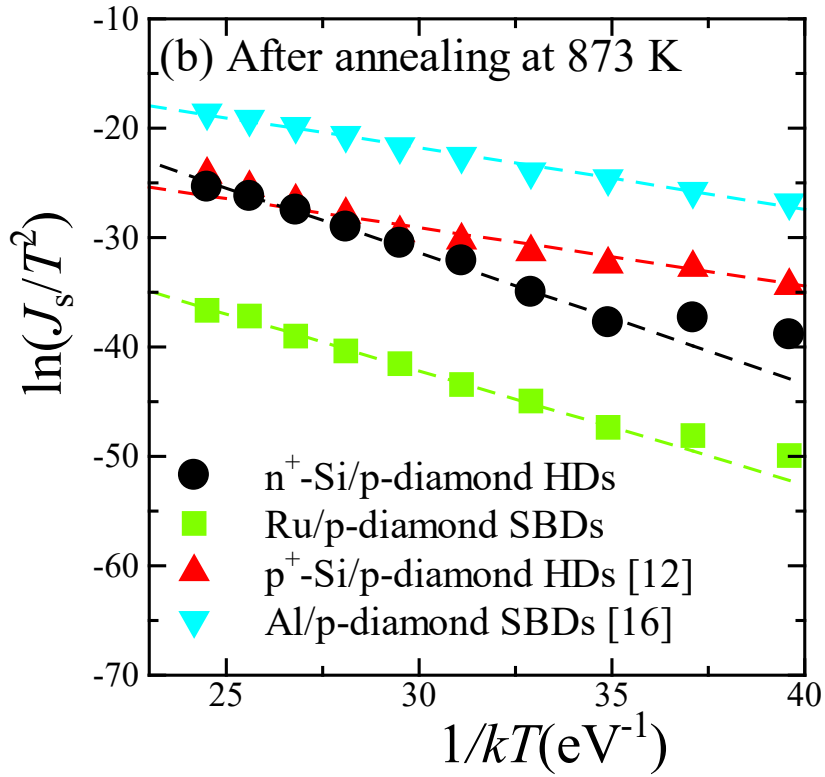
2

3

1 Fig. 4.



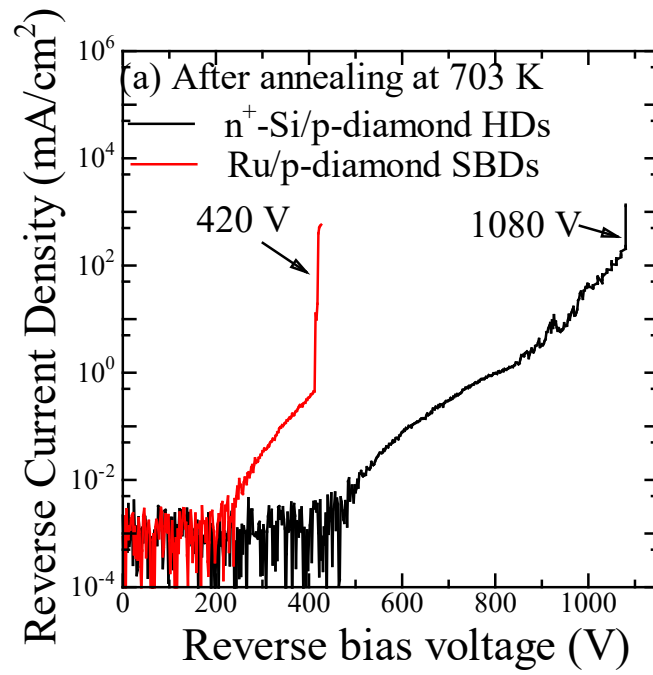
2



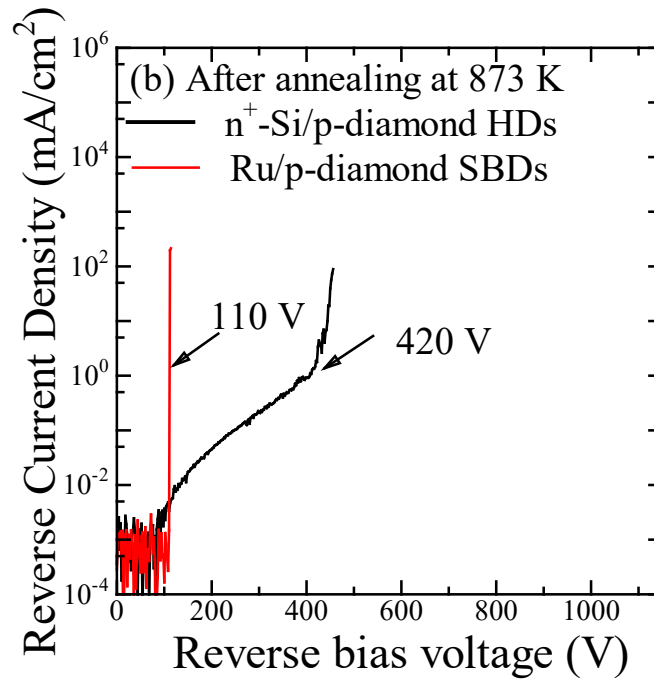
3

4

1 **Fig. 5.**

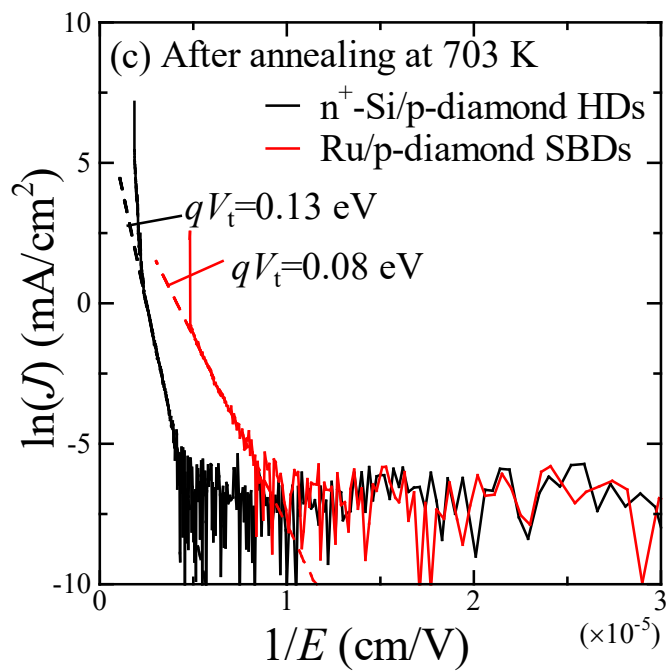


2

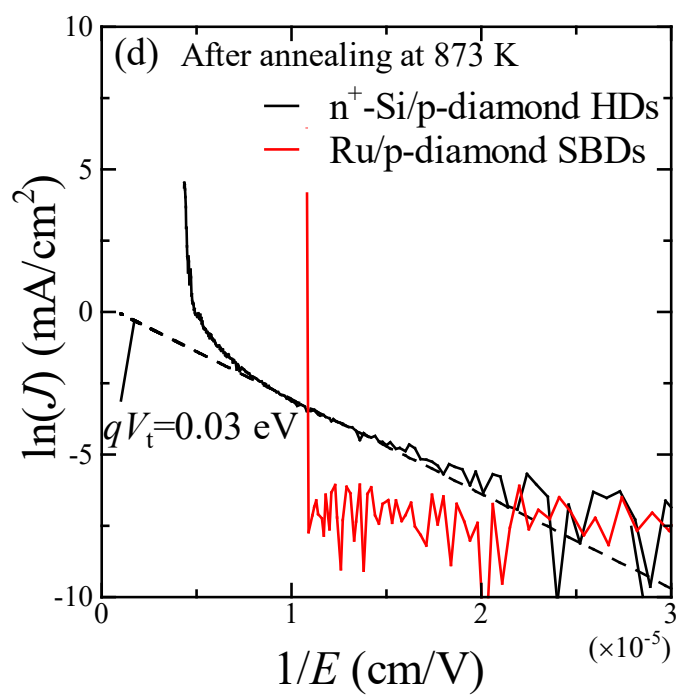


3

4



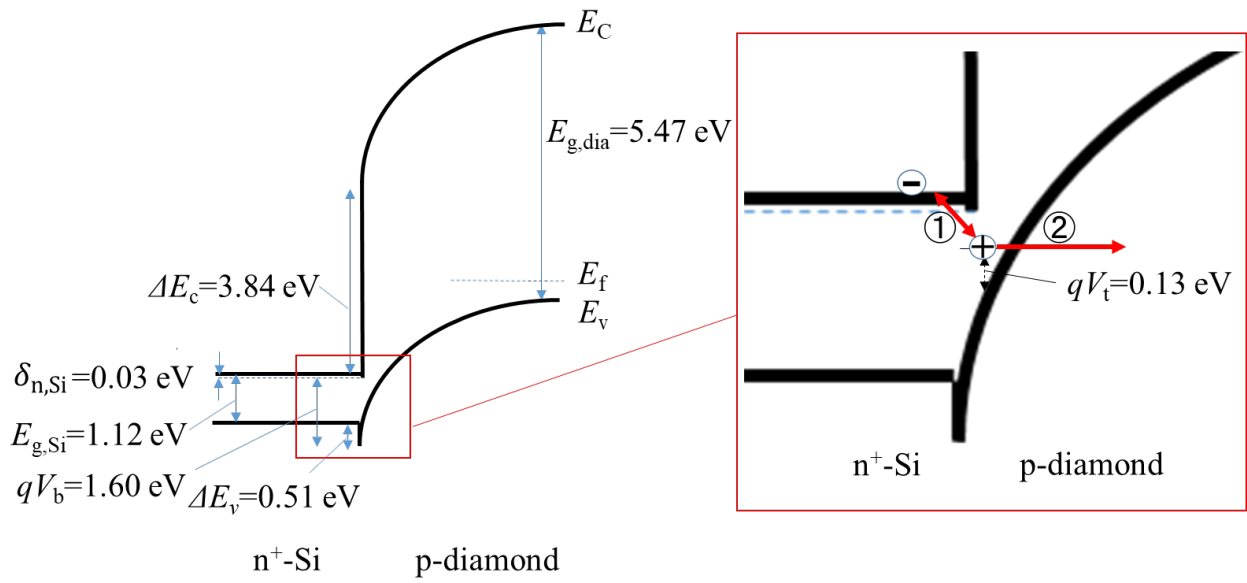
1



2

3

1 **Fig. 6.**

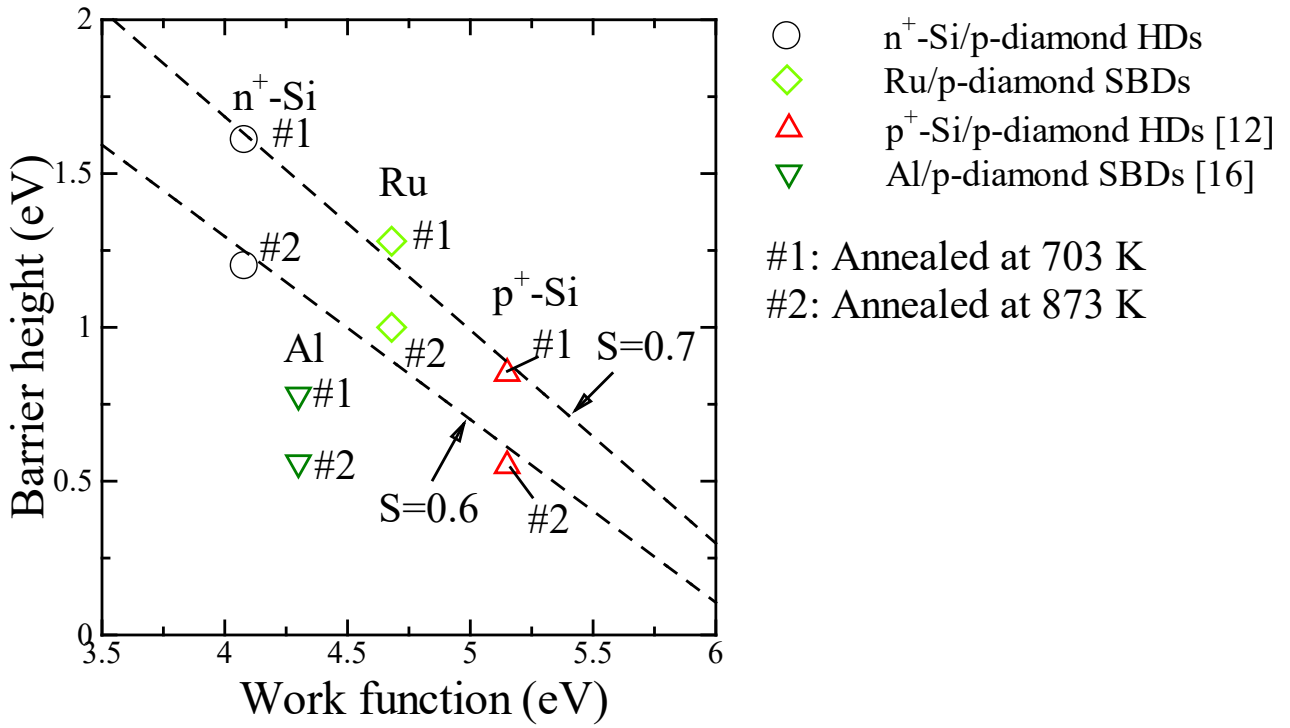


2

3

1 **Fig. 7.**

2



3

4

- 1 [1] J.Y. Tsao, S. Chowdhury, M.A. Hollis, D. Jena, N.M. Johnson, K.A. Jones, R.J. Kaplar, S. Rajan,  
2 C.G. Van de Walle, E. Bellotti, C.L. Chua, R. Collazo, M.E. Coltrin, J.A. Cooper, K.R. Evans, S.  
3 Graham, T.A. Grotjohn, E.R. Heller, M. Higashiwaki, M.S. Islam, P.W. Juodawlkis, M.A. Khan,  
4 A.D. Koehler, J.H. Leach, U.K. Mishra, R.J. Nemanich, R.C.N. Pilawa-Podgurski, J.B. Shealy, Z.  
5 Sitar, M.J. Tadjer, A.F. Witulski, M. Wraback, J.A. Simmons, Ultrawide-Bandgap Semiconductors:  
6 Research Opportunities and Challenges, *Adv. Electron. Mater.* 4 (2018) 160050.  
7 <https://doi.org/10.1002/aelm.201600501>.
- 8 [2] H. Pernegger, High mobility diamonds and particle detectors, *Phys. Status Solidi Appl. Mater. Sci.*  
9 203 (2006) 3299–3314. <https://doi.org/10.1002/pssa.200671404>.
- 10 [3] B.J. Baliga, Power Semiconductor Device Figure of Merit for High-Frequency Applications, *IEEE*  
11 *Electron Device Lett.* 10 (1989) 455–457. <https://doi.org/10.1109/55.43098>.
- 12 [4] A. Vescan, I. Daumiller, P. Gluche, W. Ebert, E. Kohn, Very high temperature operation of diamond  
13 Schottky diode, *IEEE Electron Device Lett.* 18 (1997) 556–558. <https://doi.org/10.1109/55.641444>.
- 14 [5] A. Vescan, I. Daumiller, P. Gluche, W. Ebert, E. Kohn, High temperature, high voltage operation of  
15 diamond Schottky diode, *Diam. Relat. Mater.* 7 (1998) 581–584. [https://doi.org/10.1016/s0925-](https://doi.org/10.1016/s0925-9635(97)00200-8)  
16 [9635\(97\)00200-8](https://doi.org/10.1016/s0925-9635(97)00200-8).
- 17 [6] M. Katagiri, J. Isoya, S. Koizumi, H. Kanda, Lightly phosphorus-doped homoepitaxial diamond films  
18 grown by chemical vapor deposition, *Appl. Phys. Lett.* 85 (2004) 6365–6367.

- 1 <https://doi.org/10.1063/1.1840119>.
- 2 [7] R.G. Farrer, On the substitutional nitrogen donor in diamond, *Solid State Commun.* 7 (1969) 685–  
3 688. [https://doi.org/10.1016/0038-1098\(69\)90593-6](https://doi.org/10.1016/0038-1098(69)90593-6).
- 4 [8] H. Takagi, K. Kikuchi, R. Maeda, T.R. Chung, T. Suga, Surface activated bonding of silicon wafers  
5 at room temperature, *Appl. Phys. Lett.* 68 (1998) 2222. <https://doi.org/10.1063/1.115865>.
- 6 [9] M.M.R. Howlader, T. Watanabe, T. Suga, Characterization of the bonding strength and interface  
7 current of p-Si/n-InP wafers bonded by surface activated bonding method at room temperature, *J.*  
8 *Appl. Phys.* 91 (2002) 3062–3066. <https://doi.org/10.1063/1.1430883>.
- 9 [10] T. Suga, Y. Takahashi, H. Takagi, B. Gibbesch, G. Elssner, Structure of AlAl and AlSi<sub>3</sub>N<sub>4</sub> interfaces  
10 bonded at room temperature by means of the surface activation method, *Acta Metall. Mater.* 40  
11 (1992) S133–S137. [https://doi.org/10.1016/0956-7151\(92\)90272-G](https://doi.org/10.1016/0956-7151(92)90272-G).
- 12 [11] T.H. Kim, M.M.R. Howlader, T. Itoh, T. Suga, Room temperature Cu–Cu direct bonding using  
13 surface activated bonding method, *J. Vac. Sci. Technol. A Vacuum, Surfaces, Film.* 21 (2003) 449.  
14 <https://doi.org/10.1116/1.1537716>.
- 15 [12] Y. Uehigashi, S. Ohmagari, H. Umezawa, H. Yamada, J. Liang, N. Shigekawa, Fabrication of p+–  
16 Si/p-diamond heterojunction diodes and effects of thermal annealing on their electrical properties,  
17 *Diam. Relat. Mater.* 120 (2021) 108665. <https://doi.org/10.1016/J.DIAMOND.2021.108665>.
- 18 [13] J.-H. Seo, H. Wu, S. Mikael, H. Mi, J.P. Blanchard, G. Venkataramanan, W. Zhou, S. Gong, D.

- 1 Morgan, Z. Ma, Thermal diffusion boron doping of single-crystal natural diamond, *J. Appl. Phys.* 119  
2 (2016) 205703. <https://doi.org/10.1063/1.4949327>.
- 3 [14] T. Sugino, T. Itagaki, J. Shirafuji, Formation of pn junctions by bonding of GaAs layer onto diamond,  
4 *Diam. Relat. Mater.* 5 (1996) 714–717. [https://doi.org/10.1016/0925-9635\(95\)00371-1](https://doi.org/10.1016/0925-9635(95)00371-1).
- 5 [15] P. Sittimart, S. Ohmagari, T. Matsumae, Diamond/ $\beta$ -Ga<sub>2</sub>O<sub>3</sub> pn heterojunction diodes fabricated by  
6 low-temperature direct-bonding ARTICLES YOU MAY BE INTERESTED IN, *AIP Adv.* 11 (2021)  
7 105114. <https://doi.org/10.1063/5.0062531>.
- 8 [16] Y. Uehigashi, S. Ohmagari, H. Umezawa, H. Yamada, J. Liang, N. Shigekawa, Comparison of  
9 thermal stabilities of p<sup>+</sup>-Si/p-diamond heterojunction and Al/p-diamond Schottky barrier diodes, *Jpn.*  
10 *J. Appl. Phys.* 61 (2022) SF1009. <https://doi.org/10.35848/1347-4065/AC6480>.
- 11 [17] Y. Uehigashi, S. Ohmagari, H. Umezawa, H. Yamada, J. Liang, N. Shigekawa, High temperature  
12 stability of p<sup>+</sup>-Si/p-diamond heterojunction diodes, 2021 7th Int. Work. Low Temp. Bond. 3D  
13 *Integr.* (2021) 13. <https://doi.org/10.1109/LTB-3D53950.2021.9598364>.
- 14 [18] S. Ohmagari, H. Yamada, N. Tsubouchi, H. Umezawa, A. Chayahara, S. Tanaka, Y. Mokuno, Large  
15 reduction of threading dislocations in diamond by hot-filament chemical vapor deposition  
16 accompanying W incorporations, *Appl. Phys. Lett.* 113 (2018) 032108.  
17 <https://doi.org/10.1063/1.5040658>.
- 18 [19] S. Ohmagari, H. Yamada, N. Tsubouchi, H. Umezawa, A. Chayahara, A. Seki, F. Kawaii, H. Saitoh,

- 1 Y. Mokuno, Schottky barrier diodes fabricated on diamond mosaic wafers: Dislocation reduction to  
2 mitigate the effect of coalescence boundaries, *Appl. Phys. Lett.* 114 (2019) 082104.  
3 <https://doi.org/10.1063/1.5085364>.
- 4 [20] A. Kobayashi, S. Ohmagari, H. Umezawa, D. Takeuchi, T. Saito, Suppression of killer defects in  
5 diamond vertical-type Schottky barrier diodes, *Jpn. J. Appl. Phys.* 59 (2020) SGGD10.  
6 <https://doi.org/10.7567/1347-4065/ab65b1>.
- 7 [21] J. Barjon, T. Tillocher, N. Habka, O. Brinza, J. Achard, R. Issaoui, F. Silva, C. Mer, P. Bergonzo,  
8 Boron acceptor concentration in diamond from excitonic recombination intensities, *Phys. Rev. B.* 83  
9 (2011) 073201. <https://doi.org/10.1103/PHYSREVB.83.073201/FIGURES/2/MEDIUM>.
- 10 [22] T. Teraji, S. Koizumi, Y. Koide, Ohmic contact for p-type diamond without postannealing, *J. Appl.*  
11 *Phys.* 104 (2008) 016104. <https://doi.org/10.1063/1.2936371>.
- 12 [23] T. Teraji, Y. Garino, Y. Koide, T. Ito, Low-leakage p-type diamond Schottky diodes prepared using  
13 vacuum ultraviolet light/ozone treatment, *J. Appl. Phys.* 105 (2009) 126109.  
14 <https://doi.org/10.1063/1.3153986>.
- 15 [24] J. Liang, S. Nishida, M. Arai, N. Shigekawa, Effects of thermal annealing process on the electrical  
16 properties of p<sup>+</sup>-Si/n-SiC heterojunctions, *Appl. Phys. Lett.* 104 (2014) 161604.  
17 <https://doi.org/10.1063/1.4873113>.
- 18 [25] J. Liang, S. Nishida, M. Arai, N. Shigekawa, Improved electrical properties of n-n and p-n Si/SiC

- 1 junctions with thermal annealing treatment, *J. Appl. Phys.* 120 (2016) 034504.  
2 <https://doi.org/10.1063/1.4959072>.
- 3 [26] H. Umezawa, M. Nagase, Y. Kato, S.I. Shikata, High temperature application of diamond power  
4 device, *Diam. Relat. Mater.* 24 (2012) 201–205. <https://doi.org/10.1016/J.DIAMOND.2012.01.011>.
- 5 [27] H. Okamoto, M.E. Schlesinger, E.M. Mueller, *Binary Alloy Phase Diagrams*, ASM International,  
6 2016. <https://doi.org/10.31399/ASM.HB.V03.A0006247>.
- 7 [28] O. Moutanabbir, U. Gösele, *Annu. Rev. Mater. Res.*, *Annu. Rev. Mater. Res.* 40 (2010) 469–500.  
8 <https://doi.org/10.1146/ANNUREV-MATSCI-070909-104448>.
- 9 [29] J. Liang, S. Masuya, S. Kim, T. Oishi, M. Kasu, N. Shigekawa, Stability of diamond/Si bonding  
10 interface during device fabrication process, *Appl. Phys. Express.* 12 (2019) 16501.  
11 <https://doi.org/10.7567/1882-0786/aaeedd>.
- 12 [30] N. Shigekawa, N. Watanabe, E. Higurashi, Electrical properties of Si-based junctions by SAB, *Proc.*  
13 *2012 3rd IEEE Int. Work. Low Temp. Bond. 3D Integr. LTB-3D 2012.* (2012) 109–112.  
14 <https://doi.org/10.1109/LTB-3D.2012.6238065>.
- 15 [31] M.P. Houn, Y.H. Wang, W.J. Chang, Current transport mechanism in trapped oxides: A generalized  
16 trap-assisted tunneling model, *J. Appl. Phys.* 86 (1999) 1488–1491. <https://doi.org/10.1063/1.370918>.
- 17 [32] K. Fu, J. Zhou, X. Deng, X. Qi, D.J. Smith, S.M. Goodnick, Y. Zhao, H. Fu, X. Huang, T.H. Yang,  
18 C.Y. Cheng, P.R. Peri, H. Chen, J. Montes, C. Yang, Reverse Leakage Analysis for As-Grown and

- 1 Regrown Vertical GaN-on-GaN Schottky Barrier Diodes, *IEEE J. Electron Devices Soc.* 8 (2020) 74–  
2 83. <https://doi.org/10.1109/JEDS.2020.2963902>.
- 3 [33] P.N. Volpe, J. Pernot, P. Muret, F. Omnès, High hole mobility in boron doped diamond for power  
4 device applications, *Appl. Phys. Lett.* 94 (2009) 092102. <https://doi.org/10.1063/1.3086397>.
- 5 [34] H. Surdi, F.A.M. Koeck, M.F. Ahmad, T.J. Thornton, R.J. Nemanich, S.M. Goodnick, Demonstration  
6 and Analysis of Ultrahigh Forward Current Density Diamond Diodes, *IEEE Trans. Electron Devices.*  
7 69 (2022) 254–261. <https://doi.org/10.1109/TED.2021.3125914>.
- 8 [35] A. Balducci, M. Marinelli, E. Milani, M.E. Morgada, G. Prestopino, M. Scoccia, A. Tucciarone, G.  
9 Verona-Rinati, Trapping-detrapping defects in single crystal diamond films grown by chemical vapor  
10 deposition, *Appl. Phys. Lett.* 87 (2005) 1–3. <https://doi.org/10.1063/1.2135384>.
- 11 [36] M. Werner, O. Dorsch, A. Hinze, E. Obermeier, R.E. Harper, C. Johnston, P.R. Chalker, I.M.  
12 Buckley-Golder, Space-charge-limited current flow and trap density in undoped diamond films,  
13 *Diam. Relat. Mater.* 2 (1993) 825–828. [https://doi.org/10.1016/0925-9635\(93\)90232-Q](https://doi.org/10.1016/0925-9635(93)90232-Q).
- 14 [37] P. Muret, J. Pernot, A. Kumar, L. Magaud, C. Mer-Calfati, P. Bergonzo, Deep hole traps in boron-  
15 doped diamond, *Phys. Rev. B - Condens. Matter Mater. Phys.* 81 (2010) 1–11.  
16 <https://doi.org/10.1103/PhysRevB.81.235205>.
- 17 [38] L.A. Romanko, Charge carrier trapping centers in synthetic diamond, *Diam. Relat. Mater.* 6 (1997)  
18 1674–1679. [https://doi.org/10.1016/S0925-9635\(97\)00040-X](https://doi.org/10.1016/S0925-9635(97)00040-X).

- 1 [39] M. Bruzzi, D. Menichelli, S. Sciortino, Deep levels and trapping mechanisms in chemical vapor  
2 deposited diamond ARTICLES YOU MAY BE INTERESTED IN, *J. Appl. Phys.* 91 (2002) 5765.  
3 <https://doi.org/10.1063/1.1461891>.
- 4 [40] N. Donato, N. Rouger, J. Pernot, G. Longobardi, F. Udrea, Diamond power devices: State of the art,  
5 modelling, figures of merit and future perspective, *J. Phys. D. Appl. Phys.* 53 (2020).  
6 <https://doi.org/10.1088/1361-6463/AB4EAB>.
- 7 [41] H. Umezawa, M. Nagase, Y. Kato, S.I. Shikata, Diamond vertical Schottky barrier diode with Al<sub>2</sub>O<sub>3</sub>  
8 field plate, *Mater. Sci. Forum.* 717–720 (2012) 1319–1321.  
9 <https://doi.org/10.4028/www.scientific.net/MSF.717-720.1319>.
- 10 [42] S.M. Sze, K.K. Ng, *Physics of Semiconductor Devices*, 2006. <https://doi.org/10.1002/0470068329>.
- 11 [43] A. Vescan, W. Ebert, T. Borst, E. Kohn, I V characteristics of epitaxial Schottky Au barrier diode on  
12 p<sup>+</sup> diamond substrate, *Diam. Relat. Mater.* 4 (1995) 661–665. <https://doi.org/10.1016/0925->  
13 [9635\(94\)05237-9](https://doi.org/10.1016/0925-9635(94)05237-9).
- 14 [44] H. Umezawa, T. Saito, N. Tokuda, M. Ogura, S.-G. Ri, H. Yoshikawa, S. Shikata, Leakage current  
15 analysis of diamond Schottky barrier diode, *Appl. Phys. Lett.* 90 (2007) 073506.  
16 <https://doi.org/10.1063/1.2643374>.
- 17 [45] H. Umezawa, S.I. Shikata, Leakage current analysis of diamond Schottky barrier diodes operated at  
18 high temperature, *Jpn. J. Appl. Phys.* 53 (2014) 04EP04. <https://doi.org/10.7567/JJAP.53.04EP04>.

- 1 [46] K. Ueda, K. Kawamoto, H. Asano, High-temperature and high-voltage characteristics of Cu/diamond  
2 Schottky diodes, *Diam. Relat. Mater.* 57 (2015) 28–31.  
3 <https://doi.org/10.1016/J.DIAMOND.2015.03.006>.
- 4 [47] T. Teraji, A. Fiori, N. Kiritani, S. Tanimoto, E. Gheeraert, Y. Koide, Mechanism of reverse current  
5 increase of vertical-type diamond Schottky diodes, *J. Appl. Phys.* 122 (2017) 135304.  
6 <https://doi.org/10.1063/1.4994570>.
- 7 [48] J. Liang, T. Miyazaki, M. Morimoto, S. Nishida, N. Shigekawa, Electrical properties of Si/Si  
8 interfaces by using surface-activated bonding, *J. Appl. Phys.* 114 (2013) 183703.  
9 <https://doi.org/10.1063/1.4829676>.
- 10 [49] N. Nanda Kumar Reddy, S. Godavarthi, K. Mohan Kumar, V.K. Kummara, S. V. Prabhakar  
11 Vattikuti, H.S. Akkera, Y. Bitla, S.A.K. Jilani, V. Manjunath, Evaluation of temperature dependent  
12 electrical transport parameters in Fe<sub>3</sub>O<sub>4</sub>/SiO<sub>2</sub>/n-Si metal–insulator–semiconductor (MIS) type  
13 Schottky barrier heterojunction in a wide temperature range, *J. Mater. Sci. Mater. Electron.* 30 (2019)  
14 8955–8966. <https://doi.org/10.1007/s10854-019-01223-1>.
- 15 [50] J. Liang, Y. Zhou, S. Masuya, F. Guemann, M. Singh, J. Pomeroy, S. Kim, M. Kuball, M. Kasu, N.  
16 Shigekawa, Annealing effect of surface-activated bonded diamond/Si interface, *Diam. Relat. Mater.*  
17 93 (2019) 187–192. <https://doi.org/10.1016/j.diamond.2019.02.015>.
- 18 [51] J. Liang, S. Masuya, M. Kasu, N. Shigekawa, Realization of direct bonding of single crystal diamond

- 1 and Si substrates, *Appl. Phys. Lett.* 110 (2017). <https://doi.org/10.1063/1.4978666>.
- 2 [52] H. Umezawa, K. Ikeda, R. Kumaresan, N. Tatsumi, S.I. Shikata, Increase in reverse operation limit  
3 by barrier height control of diamond schottky barrier diode, *IEEE Electron Device Lett.* 30 (2009)  
4 960–962. <https://doi.org/10.1109/LED.2009.2026439>.
- 5 [53] N.K. Reddy Nallabala, S.V.P. Vattikuti, V.K. Verma, V.R. Singh, S. Alhammadi, V.K. Kummara, V.  
6 Manjunath, M. Dhanalakshmi, V.R. Minnam Reddy, Highly sensitive and cost-effective metal-  
7 semiconductor-metal asymmetric type Schottky metallization based ultraviolet photodetecting sensors  
8 fabricated on n-type GaN, *Mater. Sci. Semicond. Process.* 138 (2022) 106297.  
9 <https://doi.org/10.1016/j.mssp.2021.106297>.
- 10 [54] N.K.R. Nallabala, S. Godavarthi, V.K. Kummara, M.K. Kesarla, D. Saha, H.S. Akkera, G.K.  
11 Guntupalli, S. Kumar, S.V.P. Vattikuti, Structural, optical and photoresponse characteristics of metal-  
12 insulator-semiconductor (MIS) type Au/Ni/CeO<sub>2</sub>/GaN Schottky barrier ultraviolet photodetector,  
13 *Mater. Sci. Semicond. Process.* 117 (2020) 105190. <https://doi.org/10.1016/j.mssp.2020.105190>.
- 14 [55] N.K.R. Nallabala, V.R.M. Reddy, V.R. Singh, K. Rahim Bakash, S. Kumar, D. Saha, V. Mahendran,  
15 V.K. Kummara, G.K. Guntupalli, S.V.P. Vattikuti, Enhanced photoresponse performance in GaN  
16 based symmetric type MSM ultraviolet-A and MIS ultraviolet-A to C photodetectors, *Sensors*  
17 *Actuators A Phys.* 339 (2022) 113502. <https://doi.org/10.1016/j.sna.2022.113502>.
- 18 [56] S. Koizumi, H. Umezawa, J. Pernot, M. Suzuki, Power Electronics Device Applications of Diamond

1 Semiconductors, Woodhead Publishing, 2018. <https://doi.org/https://doi.org/10.1016/C2016-0-03999->

2 2.

3 [57] Y.G. Chen, M. Ogura, H. Okushi, Schottky junction properties on high quality boron-doped

4 homoepitaxial diamond thin films, *J. Vac. Sci. Technol. B.* 22 (2004) 2084.

5 <https://doi.org/10.1116/1.1768186>.

6